

# Photoionization of Xe inside $C_{60}$ : Atom-fullerene hybridization, giant cross-section enhancement, and correlation confinement resonances

Mohamed E. Madjet and Thomas Renger

*Institute of Chemistry and Biochemistry, Free University, Fabeckstrasse 36a, D-14195 Berlin, Germany*

Dale E. Hopper, Matthew A. McCune, and Himadri S. Chakraborty\*

*Center for Innovation and Entrepreneurship, Department of Chemistry and Physics, Northwest Missouri State University, Maryville, Missouri 64468, USA*

Jan-M. Rost

*Max-Planck-Institut für Physik Komplexer Systeme, Nöthnitzer Strasse 38, D-01187 Dresden, Germany*

Steven T. Manson

*Department Physics and Astronomy, Georgia State University, Atlanta, Georgia 30303*

(Received 5 November 2009; published 19 January 2010)

A theoretical study of the subshell photoionization of the Xe atom endohedrally confined in  $C_{60}$  is presented. Powerful hybridization of the Xe  $5s$  state with the bottom edge of  $C_{60}$   $\pi$  band is found that induces strong structures in the  $5s$  ionization, causing the cross section to differ significantly from earlier results that omit this hybridization. The hybridization also affects the angular distribution asymmetry parameter of Xe  $5p$  ionization near the Cooper minimum. The  $5p$  cross section, on the other hand, is greatly enhanced by borrowing considerable oscillator strength from the  $C_{60}$  giant plasmon resonance *via* the atom-fullerene dynamical interchannel coupling. Beyond the  $C_{60}$  plasmon energy range the atomic subshell cross sections display confinement-induced oscillations in which, over the large  $4d$  shape resonance region, the dominant  $4d$  oscillations induce their “clones” in all degenerate weaker channels known as correlation confinement resonances.

DOI: [10.1103/PhysRevA.81.013202](https://doi.org/10.1103/PhysRevA.81.013202)

PACS number(s): 61.48.–c, 33.80.Eh, 36.40.Cg

## I. INTRODUCTION

One of the unique features of carbon fullerenes,  $C_n$ , is their internal empty space. The size of this void ranges from about a quarter of a nanometer to a few nanometers in diameter. Such structure of fullerenes intuitively implies that an atom or a molecule or a cluster or even a smaller fullerene can be stuffed into it so as to alter the molecular properties of the compound. This results in the synthesis of a brand-new family of materials—the endohedral fullerenes, more concisely the endofullerenes,  $A@C_n$  [1]. These are a very stable form of nanoscopic molecular matter that can exist even at the room temperature. Since such entrapments are easier to sustain than the traditional field entrapments, like laser cooling or magneto-optical trap, endofullerenes are unique candidates to study not only the greatly modified spectroscopy of the confined atom but also the effects of hybridization of the localized atomic electron inside the fullerene with the delocalized fullerene electrons surrounding it.

Intense research is being carried out in variedly different fields to explore applications of endofullerenes in nanotechnology. It has been shown that they can serve from being the fundamental units in designing a quantum computer [2] to the carriers of pinpoint medication delivery at the diseased human tissue [3]. Possibilities also exist for these materials to be the agents for improved superconductivity [4]. Very recently, choosing endofullerenes as the acceptor

materials in organic photovoltaic devices, a novel route toward higher power consumption efficiency is achieved [5]. The knowledge of the spectroscopy of the confined species and associated hybridization, therefore, becomes valuable to assess the potential and the limitation of such applications. From the basic science perspective, the synthesis of endofullerenes has so far not been industrial enough to spawn sufficient fundamental measurements. There however have been some recent photoabsorption experiments involving lanthanide endofullerenes using the synchrotron radiation by two groups. Measurements of the singly- and doubly-positively charged photoion yield are carried out by one group for  $Ce@C_{82}^+$  [6],  $Dy@C_{82}$  [7], and  $Pr@C_{82}$  [8]. More recently, experiments by another group has detected large modifications in the atomic  $4d$  oscillator strength distribution in  $Ce@C_{82}^+$  ion [9,10].

On the theoretical side there has been a large body of research over the past decade on the photoionization of various atomic endofullerenes. While the ionization process is treated by a number of differing many-body methods, the  $C_{60}$  shell is modeled at various levels of approximations. As for the simplest one, a Dirac delta-function type spherical attractive potential is used to model  $C_{60}$  while the ionization is treated by the random-phase approximation with exchange (RPAE) scheme. A number of calculations have emerged using this model [11]. Spherical attractive potentials of finite depth and a thickness roughly about 2.0 a.u. has also been employed to represent the  $C_{60}$  shell in other studies; the depth is calibrated by reproducing the known electron affinity of  $C_{60}$  giving a semiempirical qualification of this potential. The photoionization is treated by the RPAE method by one group [12], and

\*himadri@nwmissouri.edu

by the relativistic random-phase approximation (RRPA) by another [13]. Using a similar finite potential for  $C_{60}$  another calculation has been recently reported in RPAE by indirectly determining the continuum waves by matching at the fullerene boundaries [14]. A review of these studies is presented in Ref. [15]. All these calculations qualitatively suggest a rather ubiquitous oscillation in the ionization cross section of the confined atom that originates from the reflection of the ejected atomic electron from the cage. But, by not including the fullerene electrons, two important effects are completely omitted in these *static* model-potentials: (i) the mixing between atomic and fullerene electronic wave functions resulting in hybridization, and (ii) the dynamical effect of the collective motion of fullerene electrons on the atomic ionization.

A new type of approach, recently adopted by us, addresses these effects. Based on a model used in previous works [16,17] this approach treats all the valence electrons, four ( $2s^22p^2$ ) from each carbon atom in the fullerene, to form the delocalized charged cloud. The residual ion-core comprising of all  $C^{4+}$  ions is treated by a classical jellium shell. This approach gave a fair description of two plasmon-type collective resonances in the photoionization of empty  $C_{60}$  [18] and its singly-charged cation [19]. Using this *multielectron* description of  $C_{60}$  *ab initio* calculations for  $Ar@C_{60}$  [20] and  $Mg@C_{60}$  [21] endofullerenes have revealed remarkably strong enhancements in the photoelectron intensity from the atomic valence level which originate from the atom's dynamical coupling to the  $C_{60}$  giant plasmon resonance. We note that a simple semiclassical approach using the idea of a dynamical screening of the dielectric fullerene shell has produced a good qualitative description of the enhancement [22]. A separate attempt to account for the enhancement in Xe  $5p$  ionization of  $Xe@C_{60}$  has been made recently, although the dynamical polarizability of  $C_{60}$  is introduced in an *ad hoc* manner, since the simple delta-function model of  $C_{60}$  used in this work omits the coupling with the collective motion of the delocalized fullerene electrons [11]. It would therefore be useful to assess how much enhancement the *ab initio* calculation brings about for the  $Xe@C_{60}$  compound and how does the result compare with the existing calculation with simpler fullerene models.

Very recently our method for the multielectron description of  $C_{60}$  has predicted atom-fullerene hybrid levels in  $Xe@C_{60}$  with the consequence of dramatic structures in resulting photoionization cross sections [23]. These dimer-type states arise from the proximity between the atomic and  $C_{60}$  inner levels in contrast to the known [24] overlap-induced hybrid states near the Fermi level of smaller endofullerenes. However, how this effect might influence the ionization of neighboring channels of the system is yet to be explored. Furthermore, the ionization amplitudes of a confined atom are known to exhibit oscillations from the interference with the atomic electron's reflective emission in general, and collateral emission, i.e., emission from the delocalized part of the wave function arising from the hybridization, in particular [25]. It is also expected that the stronger atomic channel will transfer its own oscillations to a (degenerate) weaker channel over the spectral region where strong interchannel coupling is operative. Indeed, for the photoionization of  $Xe@C_{60}$ , using the static potential model for  $C_{60}$ , such an effect is recently predicted over the  $4d$  large shape resonance region where the coupling between

degenerate channels plays important role [12]. It is thus of interest to examine this effect using a multielectron description of  $C_{60}$ , particularly in the presence of the channels resulting from the hybrid states.

In this paper, the photoionization of the  $Xe@C_{60}$  endofullerene is considered. Hybrid level cross sections are compared with published results that omit the hybridization to assess the observable consequence of the effect. The effect of the hybridization on the  $5p$  photoelectron asymmetry parameter is analyzed. The enhancement of the Xe  $5p$  ionization in confinement is calculated and its dependence on the plasmon formation mechanism is uncovered. Cross sections of various atomic channels in the  $4d$  shape resonance region are analyzed to explore the interchannel transfer of oscillatory structures.

## II. GROUND STATE AND HYBRIDIZATION RESULTS

Density functional theory is used to describe the ground state electronic structure of  $Xe@C_{60}$  using the same methodology employed earlier [18,20]. The jellium potential representing 60  $C^{4+}$  ions is constructed as a uniform charge density over a spherical shell with radius  $R$  and thickness  $\Delta$ , augmented by a constant potential  $V_0$  to ensure quantitative accuracy [17].  $R$  is taken to be the known radius of  $C_{60}$ , 3.54 Å. The Xe nucleus is placed at the center of the sphere. The Kohn-Sham equations for the system of a total of 294 electrons (54 from Xe and 240 from  $C_{60}$ ) are then solved to obtain the ground state wave function in the local density approximation (LDA), and the parameters  $V_0$  and  $\Delta$  are determined by requiring both charge neutrality and obtaining the experimental value, 7.54 eV, of the first  $C_{60}$  ionization potential. This procedure yields a value of  $\Delta$  of 1.5 Å, in excellent agreement with the value inferred from experiment [26].

In addition, we include an appropriate correction to eliminate unphysical electron self-interactions for the  $i$ th subshell that render the LDA potential orbital-specific [27,28],

$$V^i(\mathbf{r}) = V_{\text{jel}}(\mathbf{r}) + \frac{Z_{\text{Xe}}}{r} + \int d\mathbf{r}' \frac{\rho(\mathbf{r}') - \rho_i(\mathbf{r}')}{|\mathbf{r} - \mathbf{r}'|} + \{V_{\text{xc}}[\rho(\mathbf{r})] - V_{\text{xc}}[\rho_i(\mathbf{r})]\}, \quad (1)$$

where the terms on the right-hand side of the equation are, respectively, the jellium-electron, Xe nucleus-electron, electron-electron direct Coulomb, and exchange-correlation potentials. As the exact form of  $V_{\text{xc}}$  is unknown in a local formalism like LDA (since the exact exchange interaction is nonlocal), we employ a widely used parametric formulation [29].

Occupied single-electron energy levels of the ground state of empty  $C_{60}$ , and the valence  $5p$  level of free Xe are shown in Fig. 1(a). Note that the harmonic oscillator notation is used for the  $C_{60}$  levels, which are classified as  $\sigma_\ell$  ( $n = 1$ ) and  $\pi_\ell$  ( $n = 2$ ) where  $\ell$  denotes the orbital angular momentum. Due to the strong delocalization of the  $C_{60}$  electrons, both  $\sigma$  and  $\pi$  levels exhibit compact energy spacings producing band-like formations. In general, all atomic levels become more loosely bound due to the Coulomb repulsion they experience from the surrounding  $C_{60}$  electron cloud, and this repulsion effect is strongest for Xe  $5p$  and  $5s$  states which are physically closest to the  $C_{60}$  shell electrons. This is seen in the position

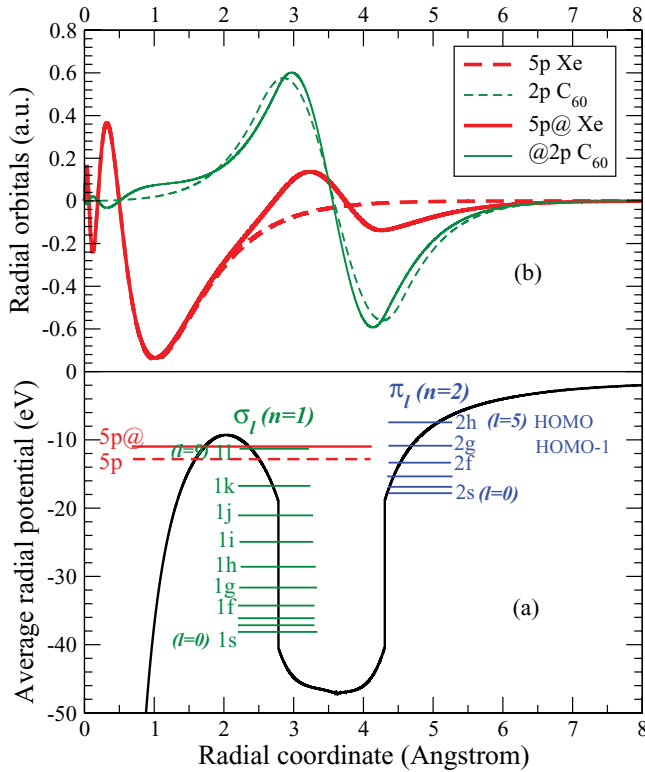


FIG. 1. (Color online) (a) The average radial LDA potential of Xe@C<sub>60</sub>.  $\pi$  ( $n = 2$ ) and  $\sigma$  ( $n = 1$ ) levels of free C<sub>60</sub>, and the valence  $5p$  level of free Xe are also shown. In addition,  $5p@$ , corresponding to the confined Xe, is displayed. (b) Radial wave functions of free Xe  $5p$  and empty C<sub>60</sub> $2p$  states, and of their counterparts,  $5p@$  and  $@2p$  in Xe@C<sub>60</sub>.

of  $-12.8$  eV of free Xe  $5p$  and  $-10.7$  eV of the confined  $5p$ , labeled as  $5p@$ , in Fig. 1(a). (We use, respectively, the symbols  $nl$  and  $nl@$  to denote levels of the free and confined atom. Likewise we use  $@nl$  to represent the level of the doped C<sub>60</sub>.) This level shift can favor or oppose the mixing mechanism between atomic and C<sub>60</sub> states that we discuss below.

Orbital mixing or hybridization may occur when two systems are joined to form a compound structure. The strength of the mixing is proportional to the wave function overlap as well as the energy proximity of the unperturbed free-system states. Since for C<sub>60</sub> a  $\pi$  orbital extends more radially inward than a  $\sigma$  orbital, the  $\pi$  orbitals induce significantly larger overlaps with the atomic valence orbitals than the  $\sigma$  orbitals. The angular momentum of participating orbitals also play an important role. For instance, Xe  $5p$  is not favored to mix with  $\pi$  states of higher angular momentum like  $d$  and above, simply because of the appearance of an effective barrier between the atom and C<sub>60</sub> from the difference of the centrifugal potentials due to the  $\ell$  mismatch. Hence Xe  $5p$  can only mix strongly with C<sub>60</sub> $2p$  and  $2s$ . However, since the Coulomb repulsion with the fullerene electrons has made Xe  $5p$  less bound, it has moved further away from C<sub>60</sub> $2p$  and  $2s$  levels [Fig. 1(a)], thereby decreasing the mixing. Also, since it is closer to  $2p$  than  $2s$ , it mixes primarily with C<sub>60</sub> $2p$ . This is seen in Fig. 1(b) where the  $5p$  of free Xe and  $2p$  of empty C<sub>60</sub> are displayed along with their mixed counterpart  $5p@$  and  $@2p$ .  $5p@$  has a

diminutive structure across the cage region, and so has  $2p@$  at the atomic region, resulting from a very weak mixing. Further, a close look reveals that  $5p@$  and  $@2p$  are the symmetric (bonding) and antisymmetric (antibonding) combinations

$$|5p@> = \sqrt{\alpha}|2p C_{60}\rangle + \sqrt{1-\alpha}|5p Xe\rangle, \quad (2a)$$

$$|@2p\rangle = \sqrt{1-\alpha}|2p C_{60}\rangle - \sqrt{\alpha}|5p Xe\rangle \quad (2b)$$

in which, since the mixing parameter  $\alpha$  is very small, the states practically retain their pure character. Similar weak mixing was also seen before in Ar  $3p@$  of the Ar@C<sub>60</sub> compound [20].

On the other hand, the Xe  $5s$  level interacts predominantly with the lowest angular momentum level  $2s$  of empty C<sub>60</sub> $\pi$  band, owing to their identical angular momentum character, as discussed above. Note that the  $5s$  level lies closely below the  $\pi$  band. Therefore, the Coulomb repulsion between the  $5s$  and the C<sub>60</sub> electrons induces a highly favorable near-degeneracy between this level and C<sub>60</sub> $2s$  by shifting the  $5s$  level close to  $2s$ . This near-degeneracy is rather accidental since the effect is exactly opposite to what the repulsion did to  $5p$  that disfavored the mixing. As a consequence, a strong hybridization results: Xe  $5s$  and C<sub>60</sub>  $2s$  states vanish in the compound system in exchange for the creation of two hybrid states of mixed Xe-C<sub>60</sub> characters. We designate the hybrid levels as  $5s2s$  and  $2s5s$ , characterizing two covalent-type Xe-C<sub>60</sub> bonds, with binding energies at  $-19.3$  eV and  $-17.5$  eV, respectively, in Fig. 2(a).

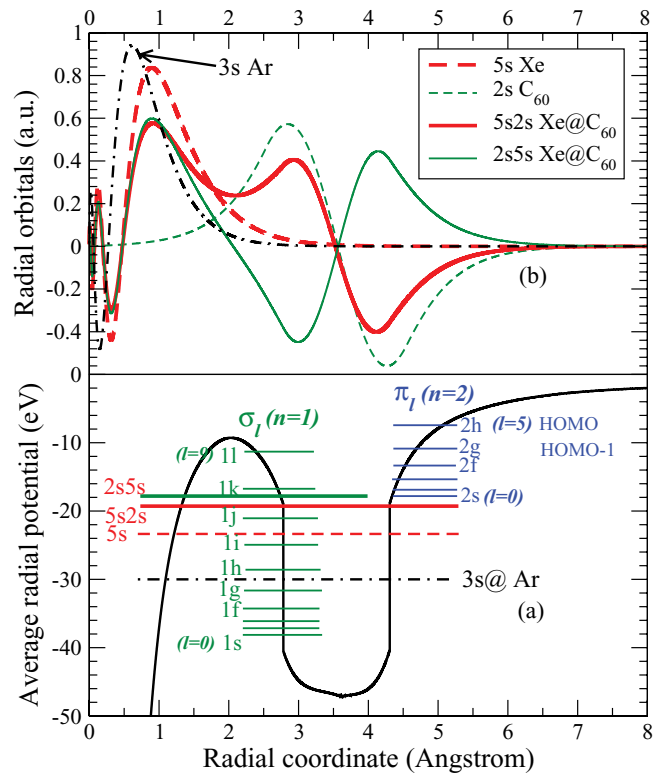


FIG. 2. (Color online) (a) The average radial LDA potential of Xe@C<sub>60</sub>.  $\pi$  ( $n = 2$ ) and  $\sigma$  ( $n = 1$ ) levels of free C<sub>60</sub>, and the  $5s$  level of free Xe is shown. Also,  $5s2s$  and  $2s5s$  hybrid levels are displayed along with the confined Ar  $3s@$  level. (b) Radial wave functions of free Xe  $5s$ , empty C<sub>60</sub> $2s$ , and the two hybrid states. The free Ar  $3s$  wave function is also shown for comparison.

The extent of hybridization is evident from the shape of the radial wave functions of the two new states in Fig. 2(b). In fact, the hybridization emerges from a nearly equal mixing and, therefore, can be described by the combinations, Eqs. (2), by considering  $\alpha = \frac{1}{\sqrt{2}}$  to yield

$$|5s2s\rangle = \frac{1}{\sqrt{2}}(|5s \text{Xe}\rangle + |2s \text{C}_{60}\rangle), \quad (3a)$$

$$|2s5s\rangle = \frac{1}{\sqrt{2}}(|5s \text{Xe}\rangle - |2s \text{C}_{60}\rangle). \quad (3b)$$

Clearly, each wave function has the probability density distributed approximately equally over the atomic and the cage region as Fig. 2(b) suggests. To compare with the situation involving a smaller noble gas atom, we also show in Fig. 2(a) the 3s level of Ar confined in C<sub>60</sub>. Note that this has a significantly large separation from the  $\pi$  band. Also, the Ar 3s radial wave function, as shown in Fig. 2(b), suggests a considerably smaller overlap with the empty C<sub>60</sub>2s orbital. These explain why no significant hybridization was seen between Ar 3s and C<sub>60</sub> [20].

For smaller fullerenes with a larger atom inside, the atomic valence orbitals overlap very strongly with the fullerene for simple geometric reason, resulting in strong admixtures. This overlap further increases for a confined open-shell atom. Indeed, covalent bondings for systems like Ce@C<sub>28</sub> [30] and Sn,Zr,U@C<sub>28</sub> [24] have already been predicted with the hybrid states forming in the vicinity of the highest occupied fullerene orbital. In contrast, the hybridization effect presented here results primarily from the energy proximity of the participating levels induced by the reduction of the binding of Xe 5s due to the repulsion force exerted by surrounding C<sub>60</sub> electrons, causing its shift toward the bottom-most level (2s) of the C<sub>60</sub> $\pi$  band.

### III. THEORETICAL TREATMENT OF PHOTOIONIZATION

A time-dependent LDA (TDLDA) approach [18] is used to calculate the dynamical response of the compound to the external dipole field  $z$ . Since the molecule is rotationally invariant, the Green's function for a parameter  $E$  can be expanded in spherical basis:

$$G(\mathbf{r}, \mathbf{r}'; E) = \sum_{lm} G_{lm}(r, r'; E) Y_{lm}^*(\Omega) Y_{lm}(\Omega'), \quad (4)$$

where the radial component  $G_{lm}(r, r'; E)$  satisfies the radial equation

$$\left( \frac{1}{r^2} \frac{\partial}{\partial r} r^2 \frac{\partial}{\partial r} - \frac{\ell(\ell+1)}{r^2} - V_{\text{LDA}} + E \right) G_{lm}(r, r'; E) = \frac{\delta(r-r')}{r^2}. \quad (5)$$

$G_{lm}$  is constructed with homogeneous solutions  $j_l(r; E)$  and  $h_l(r; E)$  of (5), satisfying boundary conditions at  $r = 0$  and  $r = \infty$ , respectively, as

$$G_{lm}(r, r'; E) = \frac{j_l(r_{<}; E) h_l(r_{>}; E)}{W[j_l, h_l]}, \quad (6)$$

where the Wronskian

$$W[j, h] = r^2 [j(r) dh(r)/dr - dj(r)/dr h(r)]_{r=c} \quad (7)$$

and is independent of the arbitrary constant  $c$ . Using the Green's function, the independent particle (IP) susceptibility is then constructed by the ground state single-electron orbitals  $\phi_i$  and energies  $\epsilon_i$  as

$$\chi_0(\mathbf{r}, \mathbf{r}'; \omega) = \sum_i \phi_i^*(\mathbf{r}) \phi_i(\mathbf{r}') G(\mathbf{r}, \mathbf{r}'; \epsilon_i + \hbar\omega) + \sum_i \phi_i(\mathbf{r}) \phi_i^*(\mathbf{r}') G^*(\mathbf{r}, \mathbf{r}'; \epsilon_i - \hbar\omega), \quad (8)$$

where the index  $i$  runs over the occupied states only.

The external perturbation  $z$  representing the dipole interaction of electrons with the linearly polarized light, induces a frequency-dependent complex change in the electron density. This can, in principle, be written as

$$\delta\rho(\mathbf{r}; \omega) = \int \chi(\mathbf{r}, \mathbf{r}'; \omega) z' d\mathbf{r}', \quad (9)$$

where the full susceptibility  $\chi$  incorporates the dynamical electron correlation. Using instead the IP susceptibility [Eq. (8)], the induced density can, equivalently, be written as

$$\delta\rho(\mathbf{r}; \omega) = \int \chi_0(\mathbf{r}, \mathbf{r}'; \omega) \delta V(\mathbf{r}'; \omega) d\mathbf{r}', \quad (10)$$

in which

$$\delta V(\mathbf{r}'; \omega) = z + \int \frac{\delta\rho(\mathbf{r}'; \omega)}{|\mathbf{r} - \mathbf{r}'|} d\mathbf{r}' + \left[ \frac{\partial V_{\text{xc}}}{\partial \rho} \right]_{\rho=\rho_0} \delta\rho(\mathbf{r}; \omega), \quad (11)$$

where the second and third term on the right-hand side are, respectively, the induced change of the Coulomb and the exchange-correlation potentials. Obviously, besides including the external perturbation  $z$ ,  $\delta V$  incorporates the dynamical field produced through many-electron interactions and, thereby, plays the role of an effective perturbation to the molecule.

$\chi$  is related to  $\chi_0$  by the matrix equation

$$\chi = \chi_0 \left[ 1 - \frac{\partial V}{\partial \rho} \chi_0 \right]^{-1}, \quad (12)$$

involving the variation of ground state potential  $V$  with respect to the ground state density  $\rho$ . Equation (12) can be solved for  $\chi$  using the matrix inversion method [31].  $\delta\rho$  and, hence,  $\delta V$  can then be directly obtained via Eqs. (9) and (11), respectively.

The photoabsorption cross section is then finally evaluated in terms of  $\delta V$  as

$$\sigma_{\text{PA}}(\omega) = 4\pi^2 \gamma \omega \sum_{i,j} f_i (1 - f_j) | \langle j | \delta V(\mathbf{r}'; \omega) | i \rangle |^2 \times \delta(\hbar\omega - \epsilon_j + \epsilon_i), \quad (13)$$

where  $\delta V(\mathbf{r}'; \omega) = \delta V(r'; \omega) Y_{10}(\Omega)$  to validate the dipole selection and  $f_i$  are Fermi occupation factors. Clearly, the index  $j$  scans the complete set of single-electron excited as well as continuum states. Setting  $i$  to an occupied bound state ( $n\ell$ ) and  $j$  to the allowed continuum states ( $k\ell'$ ), one can derive a formal expression for the photoionization cross section as the sum of independent subshell cross sections  $\sigma_{n\ell \rightarrow k\ell'}$ ,

corresponding to a dipole transition  $n\ell \rightarrow k\ell'$ ,

$$\sigma_{\text{PI}}(\omega) = \sum_{n\ell} \sigma_{n\ell \rightarrow k\ell'} \sim \sum_{n\ell} 2(2\ell + 1) |\langle \phi_{k\ell'} | \delta V | \phi_{n\ell} \rangle|^2. \quad (14)$$

The radial component  $P_{k\ell}$  of the final continuum wave function  $\phi_{k\ell}$  has the appropriate asymptotic behavior:

$$\lim_{r \rightarrow \infty} P_{k\ell}(r) \sim \lim_{r \rightarrow \infty} [\cos(\delta_\ell) F_\ell(kr) + \sin(\delta_\ell) G_\ell(kr)] \\ = \sin\left(kr - \frac{1}{2}\pi + \frac{z}{k} \ln(2kr) + \zeta_\ell + \delta_\ell\right), \quad (15)$$

where  $F_\ell$  and  $G_\ell$  are respectively the regular and irregular spherical Coulomb functions, and  $\zeta_\ell = \arg \Gamma(\ell + 1 - iz/k)$  is the Coulomb phase-shift associated with the asymptotic charge  $z$  seen by the ejected electron.

Obviously, replacing  $\delta V$  by  $z$  in Eqs. (13) and (14), we find the independent particle (IP) LDA results of the absorption and ionization cross sections, respectively.

## IV. PHOTOIONIZATION RESULTS AND DISCUSSION

### A. Ionization of hybrid levels

Photoionization cross sections of the two Xe-C<sub>60</sub> hybrid states,  $5s2s$  and  $2s5s$ , are presented in Fig. 3(a). Since the hybridization is a ground state effect that alters the initial wave functions, the independent particle LDA results already show rich oscillatory structures. As the hybrid orbitals spread almost equally over the Coulomb (atomic) and the C<sub>60</sub> regions

[Fig. 2(b)], oscillations originate from two separate effects [25]. First, the outgoing direct ionization amplitude from the atomic region interferes with two reflected amplitudes from the inner and outer radii of the cage-wall. This interference however exists for the ionization from any arbitrary subshell of a confined atom. The second effect, special for a hybrid state, is the interference of the direct amplitude with the electron ejected from inside the cage-wall itself driven by the force from the rapid radial variations of the potential at the wall-edges. This later effect must be strong since the hybrid states have significant electron probability density around the cage-wall. In general, the LDA curves in Fig. 3(a) are very similar to each other in structure except for a shallower second minimum in  $5s2s$  at 72 eV, while for  $2s5s$  this structure is very sharp appearing at a lower energy (47 eV).

Figure 3(a) also displays the TDLDA results for the hybrid states. Inclusion of the interchannel coupling in TDLDA results in three effects: (i) Narrow single-electron autoionizing resonances appear. Up until 37 eV these spikes correspond to Xe  $5p \rightarrow ns, nd$  excitations plus all possible dipole-allowed excitations in C<sub>60</sub> degenerate with the hybrid level continua. Spikes corresponding to the excitations from inner levels,  $4d@$ ,  $4p@$ , and  $4s@$ , appear just before the ionization thresholds (shown) of these levels. (ii) In addition, below the Xe  $4d@$  threshold the coupling of the hybrid state channels with the C<sub>60</sub> channels via TDLDA induces a strong increase in the hybrid state cross sections as seen in Fig. 3(a). This occurs owing to the following. The free C<sub>60</sub> cross section (shown) is very large in this region due to the onset of two collective plasmon resonances centered at 16.5 and 38 eV. Since each hybrid wave function has about one-half of its probability density located within the C<sub>60</sub> shell region, it overlaps significantly with the C<sub>60</sub> orbitals. As a consequence, the hybrid state photoionization matrix elements experience considerable increment  $\Delta D$ , that, using the Fano formalism [32], can be expressed as

$$\Delta D(E) = \sum_{n\ell} \int dE' \frac{\langle \psi_{n\ell}(E') | \frac{1}{|r-r_{n\ell}} | \psi(E) \rangle}{E - E'} D_{n\ell}(E'), \quad (16)$$

where the numerator is a measure of the overlaps, since  $\psi$  and  $\psi_{n\ell}$  are, respectively, the hybrid and C<sub>60</sub> continuum-channel wave functions, and  $D_{n\ell}$  represents all the C<sub>60</sub> LDA matrix elements. Note in Fig. 3(a) that for the  $2s5s$  cross section TDLDA (which includes this coupling) induces about an order of magnitude increase in the cross section near the peaks of each plasmon resonance. (iii) Finally, above the Xe  $4d@$  ionization threshold the free C<sub>60</sub> cross section considerably weakens and hence a different mechanism plays out from the coupling with strong  $4d@$  cross section (shown) that displays the well-known shape resonance. In general, for free Xe the  $4d$  shape resonance influences resonance structures in all degenerate weaker channels owing to the interchannel coupling. And since the hybrid wave functions have about 50% of their probability density in the atomic region, they should also participate in this coupling, leading to modifications in the results when obtained by TDLDA. This is seen by the comparison between the LDA and TDLDA cross sections for the hybrid states above the  $4d@$  threshold in Fig. 3(a). Enhancements occur below 124 eV and above 124 eV the

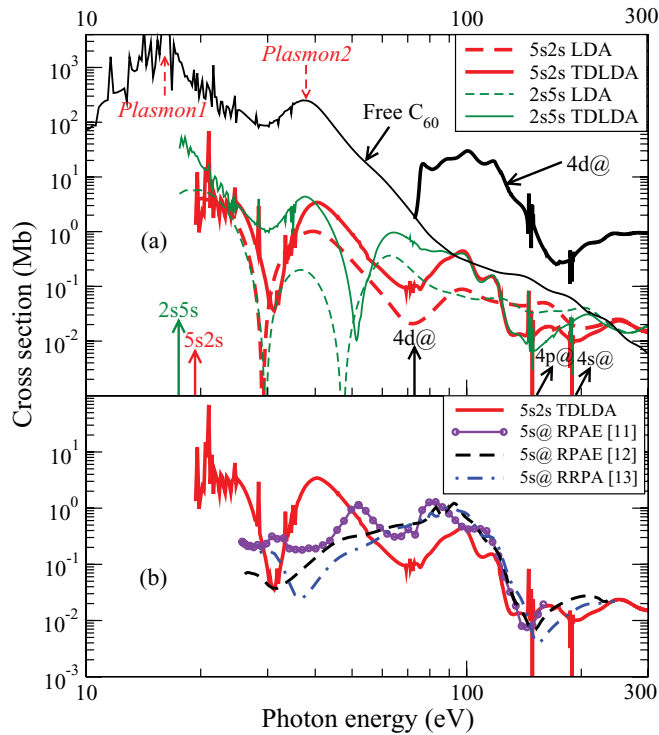


FIG. 3. (Color online) (a) LDA and TDLDA photoionization cross sections for the hybrid states  $5s2s$  and  $2s5s$ . Total free C<sub>60</sub> and Xe  $4d@$  cross sections, both in TDLDA, are also shown. The various ionization thresholds are indicated. (b)  $5s2s$  TDLDA cross section compared with earlier results [11–13] ( $5s@$ ) that omit the hybridization effect.

TDLDA curves are pushed down, reflecting the effect of a Cooper minimum in the  $4d@$  cross section at about 175 eV.

In Fig. 3(b) the  $5s2s$  hybrid state cross section is compared with previous results that are calculated by employing the  $\delta$ -function-type [11] and static-potential-type [12,13] models which omit the Xe- $C_{60}$  hybridization phenomenon that our method includes. As seen, while results from these simple models are in fair accord with each other, sharp disagreements are noted between them and the present result below 100 eV; and even above 100 eV there remain significant differences (note the logarithmic scale). This emphasizes the important consequence of the hybridization and stresses the need for a multielectron description of  $C_{60}$ .

### B. Ionization of valence $5p$ level

Photoionization cross sections for the valence  $5p$  level of free Xe and confined Xe ( $5p@$ ) calculated in TDLDA are shown in Fig. 4(a). In the  $C_{60}$  collective resonance (plasmon) region, below 40 eV photon energy that is, remarkable modifications of the  $5p$  cross section as a result of the confinement emerge. The most dramatic enhancement occurs around 17 eV, the position of the  $C_{60}$  giant plasmon. Going higher in energy, a relatively weaker shoulder-like structure appears between 24 eV and 40 eV. Beyond 40 eV, however, the  $5p@$  cross section is seen to oscillate about the (free Xe)  $5p$  result. Similar enhancements have been found previously for the valence ionizations of confined atoms of smaller sizes, namely,  $3p@$  of Ar [20] and  $3s@$  of Mg [21].

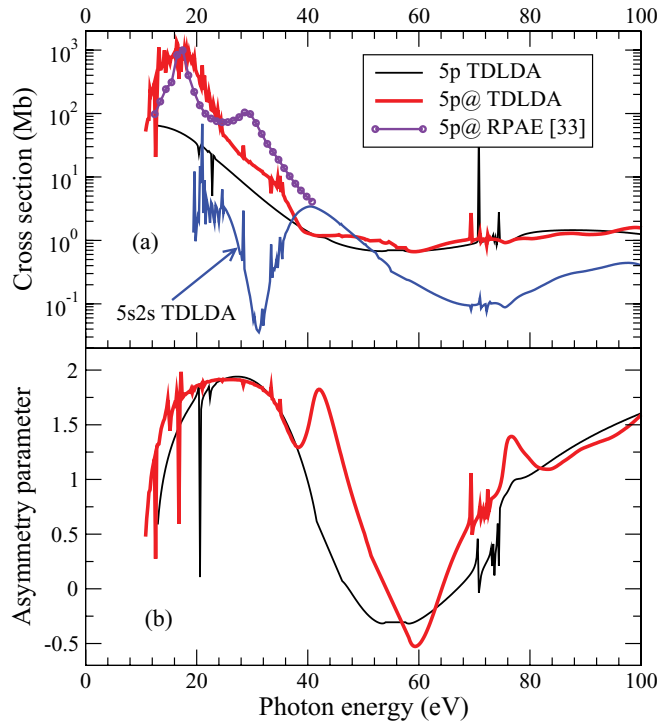


FIG. 4. (Color online) (a) TDLDA cross sections for the outer  $5p$  subshell of free ( $5p$ ) and confined ( $5p@$ ) Xe. The hybrid  $5s2s$  TDLDA cross section is also shown along with the RPAE result from Ref. [33]. (b)  $5p$  TDLDA angular distribution asymmetry parameter for free and confined Xe.

The underlying reason for this enhancement is the transfer of oscillator strength from the  $C_{60}$  ionization channels to the atomic  $5p$  channel through the atom-fullerene dynamical coupling. To scrutinize the mechanism we can resort back to Eq. (16) that will now represent the leading order correction to the Xe  $5p$  photoamplitude owing to its interaction with a number of  $C_{60}$  channels  $n\ell$ . Since the  $5p@$  wave function overlaps somewhat with the  $C_{60}$  wave functions [Fig. 1(b)] due to a weak mixing, this correction term must be nonvanishing. But why is the correction so strikingly huge as seen in Fig. 4(a)? This is due to the following reason. The existence of two plasmon resonances in free  $C_{60}$  implies that a coherent mixing of various  $C_{60}$  dipole matrix elements forms two regions of constructive interference via a mechanism of *phase-coherent* interchannel coupling [18]. Since the  $5p@$  ionization channel opens approximately at the onset of the low energy (giant) plasmon, it must also participate in the process. Indeed, the correction terms add up coherently, leading to the dramatic enhancement in the low energy plasmon region. The higher-energy shoulder structure is a combined effect of the higher energy plasmon in the  $C_{60}$  channel and a subsequent suppression due to the Cooper minimum existing in the Xe  $5p$  channel. The transfer of the oscillator strength from the  $C_{60}$  channels to the Xe  $5p$  channel can be quantified by comparing the oscillator strength values, 5.1 and 62.8, that the  $5p$  and  $5p@$  cross sections exhaust in the energy range from the ionization threshold to 40 eV.

The  $5p$  cross section of Xe confined in  $C_{60}$  has also been calculated recently using the  $\delta$ -function modeling of  $C_{60}$  [33] which we also present in Fig. 4(a). As seen, except only for the peak position of the low energy enhancement this result does not really agree with the present result. In Ref. [33], the polarization effect of  $C_{60}$  on the central atom is incorporated by inserting a multiplicative factor in an ad hoc manner which is expressed as a function of the dynamical polarizability of  $C_{60}$  determined by the sum rule considerations making use of the experimental photoeffect cross section data. This factor modified the cross section and enhanced a confinement-induced oscillation at about 17 eV region to produce the giant structure. However, in a linear response theory, like TDLDA, the dynamical effect of  $C_{60}$  on the  $5p@$  amplitude can be expressed as the sum of the single electron (SE) and the collective electron (CE) amplitudes. Referring to Eqs. (11) and (14) these amplitudes are, respectively,

$$\langle SE \rangle \sim \langle \phi_{k\ell'} | z | \phi_{5p@} \rangle, \quad (17a)$$

$$\langle CE \rangle \sim \langle \phi_{k\ell'} | \delta V' | \phi_{5p@} \rangle. \quad (17b)$$

Here

$$\delta V' = \int \frac{\delta \rho(\mathbf{r}'; \omega)}{|\mathbf{r} - \mathbf{r}'|} d\mathbf{r}' + \left[ \frac{\partial V_{xc}}{\partial \rho} \right]_{\rho=\rho_0} \delta \rho(\mathbf{r}; \omega). \quad (18)$$

Obviously, the cross section  $\sigma_{5p@}$ , which is the coherent superposition of these amplitudes, can be written as

$$\sigma_{5p@} \sim |\langle SE \rangle|^2 + |\langle CE \rangle|^2 + [\langle SE \rangle \langle CE \rangle^* + \langle SE \rangle^* \langle CE \rangle], \quad (19)$$

where the terms in the square bracket are the interference contributions. Clearly, in the low-energy region where the collective motion is very large  $|\langle CE \rangle|^2$  dominates, while in

the high-energy region where the collective motion practically vanishes  $|\langle SE \rangle|^2$  rules; the dynamics at 17 eV must be an almost *pure* collective contribution. Only in the decaying part of each plasmon do the interference terms become important. This is why the ansatz used in Ref. [33] where the enhancement in  $5p@$  cross section is generated by multiplying by a polarization factor cannot be correct. Note further that, even at 30 eV, the ansatz gives a  $5p@$  cross section almost an order of magnitude larger than the present TDLDA result.

The  $5p$  and  $5p@$  angular distribution asymmetry parameters calculated in TDLDA are shown in Fig. 4(b). The angular distribution is calculated from the ratio of the amplitudes of the dipole channels  $p \rightarrow s, d$ . Note that near the 17 eV region the angular distribution sees some increment effect from the confinement, but it is far weaker than the effect in the cross section in Fig. 5(a). This is because even if the ionization amplitudes are considerably increased at 17 eV, their ratio neutralizes the effect to a large extent. However, the comparison of  $5p$  and  $5p@$  results suggests significant modification in the angular distribution profile from the confinement in the energy range 40–60 eV. This happens owing to the existence of the  $5p$  Cooper minimum in this region. As a matter of fact, since the Cooper minimum is in the  $5p \rightarrow d$  channel, only the  $5p \rightarrow s$  channel remains, leading to an isotropic angular distribution,  $\beta = 0$ . Therefore, the Cooper minimum is located where  $\beta = 0$ , which occurs at about 47 eV for  $5p$ , but at about 54 eV for  $5p@$ , as seen in Fig. 4(b). This shift in the location of the Cooper minimum is due primarily

to interchannel coupling with the  $5s$  channels. Specifically, the  $5s2s$  and  $2s5s$  hybrid state amplitudes become stronger in this region [the  $5s2s$  cross section is shown in Fig. 4(a)] and modify the much weaker  $5p@ \rightarrow d$  amplitude through interchannel coupling. This interchannel coupling is not strong enough to affect the  $5p@ \rightarrow s$  channel, however. Thus, since the cross section is  $5p@ \rightarrow s$  channel in the Cooper minimum region, the  $5p@$  cross section is hardly affected. Note that the effect is in essence an indirect dynamical impact of the hybridization.

### C. Ionization in the $4d$ shape resonance region

For the photoionization of free Xe, a large shape resonance is created above the  $4d$  threshold from the  $4d \rightarrow kf$  channel. The  $4d$  photoionization cross section is much larger than the degenerate  $5p$  and  $5s$  cross sections of the free Xe in the resonance region. Consequently, significant interchannel couplings of  $5p$  and  $5s$  with  $4d$  kick in that induce resonance structures also in the  $5p$  and  $5s$  channels which appear like smaller replicas of the resonance in the  $4d$  channel. This interchannel coupling, when Xe is confined in C<sub>60</sub>, produces dramatic effects.

Figure 5(a) shows the free Xe  $4d$  cross section calculated in LDA that displays a sharp structure immediately above the threshold from the strong centrifugal barrier effect of the  $4d$  electron. The LDA  $4d@$  result, also shown in Fig. 5(a), is seen to simply oscillate around the  $4d$  result as expected. The LDA curves for other degenerate channels, namely,  $5p@$ ,  $5s2s$ , and  $2s5s$ , for the confined Xe (shown) exhibit similar oscillations. The TDLDA method, that includes the interchannel coupling, pushes down, broadens, and blue-shifts to 100 eV the sharp structure in LDA  $4d$ , and thereby provides the true shape of the resonance as presented in Fig. 5(b) for the free Xe. The TDLDA  $4d@$ , as seen in Fig. 5(b), has the average shape of the free result, plus the superimposed oscillations from the confinement. Note that for both LDA and TDLDA the largest oscillation occurs at the maximum of the corresponding free cross section, since the amplitude of the oscillations are proportional to the magnitude of the corresponding free atomic cross section [25].

What transpires for the shape of the TDLDA cross sections of  $5p@$ ,  $5s2s$ , and  $2s5s$  channels, shown in Fig. 5(b), is however remarkable. Strong couplings enable the  $4d@$  channel to etch out some of its own oscillations in the cross sections of these weaker channels. In particular, the structures at 100 eV and 117 eV are the most prominent ones which appear in all the curves, seen in Fig. 5(b). This transfer of confinement resonance oscillations from  $4d@$  to  $5s@$  in the  $4d$  shape resonance region was predicted recently in a calculation that uses a static model of C<sub>60</sub> [12] and termed correlation confinement resonances. The present results reveal that in a more realistic multielectron treatment of C<sub>60</sub> where  $5s$  loses its atomic identity the effect still persists. It further shows that the effect influences the outermost  $5p@$  ionization also.

## V. CONCLUSION

A detailed theoretical study of the photoionization of Xe endohedrally sequestered in C<sub>60</sub> has been carried out. Strong

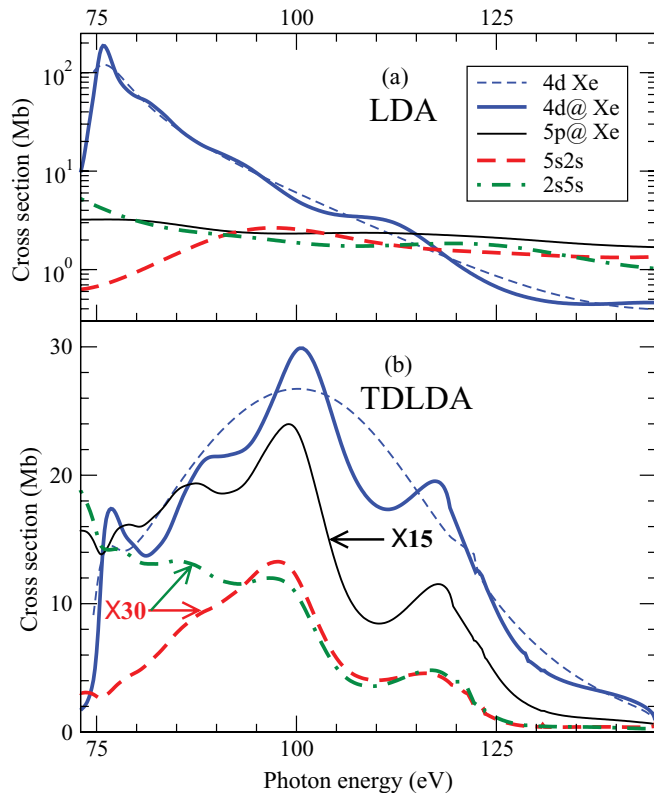


FIG. 5. (Color online) LDA (a) and TDLDA (b) cross sections of free ( $4d$ ) and confined ( $4d@$ ) Xe  $4d$ , confined Xe  $5p$ , and the hybrid states  $5s2s$  and  $2s5s$  over the  $4d$  shape resonance region.  $5p@$ ,  $2s5s$ , and  $5s2s$  results are scaled up to aid the comparison.

atom-fullerene hybridization is shown to occur between the Xe  $5s$  and the bottom-most  $\pi$  level of  $C_{60}$ . The effect emerges due to the reduction of the  $5s$  electron binding energy from the repulsion experienced from the  $C_{60}$  delocalized electrons which moves the level close enough to the bottom of the  $\pi$  band to induce a ground state (static) coupling from the near-degeneracy. The mixed character of these hybrid levels produces particularly interesting ionization behaviors. The strength of the predicted cross sections are comparable to those of a pure atomic state making them amenable to possible measurements. In addition, the coexisting delocalized character of the hybrids engenders rich oscillatory structures in the cross section.

A huge boost in the outer valence  $5p$  cross section of Xe under confinement is uncovered and shown to be due to an atom-fullerene dynamical coupling that moves a large amount of oscillator strength from the  $C_{60}$  ionization to the atomic ionization in the spectral region of  $C_{60}$  collective electron motions. However, this phenomenon only slightly influences the  $5p$  angular distribution. But, in the vicinity of the  $5p$  Cooper minimum it is found that the  $5p$  angular distribution is

greatly affected by the two nearby hybrid channels, pointing out a collateral consequence of the hybridization.

Finally, in the region of the atomic  $4d$  shape resonance electron correlation in the form of interchannel coupling is shown to enable the strong and oscillatory  $4d$  cross section of confined Xe to transfer two of its oscillations to all other open channels of Xe, including those of the hybridized states. This embodies another case of correlation confinement resonances, where the oscillations in the cross section resulting from the interference of continuum waves corresponding to direct ejection, and those reflected from the confining wall being transferred not only to other degenerate (but weaker) atomic photoionization channels, but to  $C_{60}$  photoionization channels as well.

#### ACKNOWLEDGMENTS

The work is supported by NSF and DOE, Basic Energy Sciences. M.E.M. and T.R. acknowledge the support from CoE UniCat coordinated by TU Berlin and funded by Deutsche Forschungsgemeinschaft.

- 
- [1] L. Dunsch and S. Yang, *Small* **3**, 1298 (2007).  
 [2] W. Harneit, C. Boehme, S. Schaefer, K. Huebner, K. Fostiropoulos, and K. Lips, *Phys. Rev. Lett.* **98**, 216601 (2007).  
 [3] J. B. Melanko, M. E. Pearce, and A. K. Salem, in *Nanotechnology in Drug Delivery*, edited by M. M. de Villiers, P. Aramwit, and G. S. Kwon (Springer, New York, 2009), p. 105.  
 [4] A. Takeda, Y. Yokoyama, S. Ito, T. Miyazaki, H. Shimotani, K. Yakigaya, T. Kakiuchi, H. Sawa, H. Takagi, K. Kitazawa, and N. Dragoe, *Chem. Commun.* **8**, 912 (2006).  
 [5] R. B. Ross, C. M. Cardona, D. M. Guldi, S. G. Sankaranarayanan, M. O. Reese, N. Kopidakis, J. Peet, B. Walker, G. C. Bazan, E. V. Keuren, B. C. Holloway, and M. Drees, *Nat. Mater.* **8**, 208 (2009).  
 [6] K. Mitsuke, T. Mori, and J. Kou, *J. Chem. Phys.* **122**, 064304 (2005).  
 [7] K. Mitsuke, T. Mori, J. Kou, Y. Haruyama, Y. Takabayashi, and Y. Kubozono, *Int. J. Mass Spectrom.* **243**, 121 (2005).  
 [8] H. Katayanagi, B. Kafle, J. Kou, T. Mori, K. Mitsuke, Y. Takabayashi, E. Kuwahara, and Y. Kubozono, *J. Quant. Spectrosc. Radiat. Transfer* **109**, 1590 (2008).  
 [9] A. Müller, S. Schippers, M. Habibi, D. Esteves, J. C. Wang, R. A. Phaneuf, A. L. D. Kilcoyne, A. Aguilar, and L. Dunsch, *Phys. Rev. Lett.* **101**, 133001 (2008).  
 [10] A. Müller, S. Schippers, R. A. Phaneuf, M. Habibi, D. Esteves, J. C. Wang, A. L. D. Kilcoyne, A. Aguilar, S. Yang, and L. Dunsch, *J. Phys: Conf. Ser.* **88**, 012038 (2007).  
 [11] M. Ya. Amusia, A. S. Balenkov, and L. V. Chernycheva, *J. Phys. B* **41**, 165201 (2008), and references therein.  
 [12] V. K. Domatov and S. T. Manson, *J. Phys. B* **41**, 165001 (2008), and references therein.  
 [13] K. Govil, A. J. Siji, and P. C. Deshmukh, *J. Phys. B* **42**, 065004 (2009), and references therein.  
 [14] Z. Chen and A. Z. Msezane, *J. Phys. B* **42**, 165206 (2009).  
 [15] V. K. Dolmatov, in *Advances in Quantum Chemistry. Theory of Confined Quantum Systems*, edited by J. R. Sabin and E. Brändas (Academic Press, New York, 2009), Vol. 58, p. 13ff.  
 [16] G. Wendin and B. Wästberg, *Phys. Rev. B* **48**, 14764 (1993).  
 [17] M. J. Puska and R. M. Nieminen, *Phys. Rev. A* **47**, 1181 (1993); **49**, 629 (1994).  
 [18] M. E. Madjet, H. S. Chakraborty, J. M. Rost, and S. T. Manson, *J. Phys. B* **41**, 105101 (2008).  
 [19] S. W. J. Scully, E. D. Emmons, M. F. Gharaibeh, R. A. Phaneuf, A. L. D. Kilcoyne, A. S. Schlachter, S. Schippers, A. Müller, H. S. Chakraborty, M. E. Madjet, and J. M. Rost, *Phys. Rev. Lett.* **94**, 065503 (2005).  
 [20] M. E. Madjet, H. S. Chakraborty, and S. T. Manson, *Phys. Rev. Lett.* **99**, 243003 (2007).  
 [21] H. S. Chakraborty, M. E. Madjet, Jan-M. Rost, and S. T. Manson, *Phys. Rev. A* **78**, 013201 (2008).  
 [22] S. Lo, A. V. Korol, and A. V. Solov'yov, *Phys. Rev. A* **79**, 063201 (2009).  
 [23] H. S. Chakraborty, M. E. Madjet, T. Renger, Jan-M. Rost, and S. T. Manson, *Phys. Rev. A* **79**, 061201(R) (2009).  
 [24] K. Jackson, E. Kaxiras, and M. R. Pederson, *J. Phys. Chem.* **98**, 7805 (1994).  
 [25] M. A. McCune, M. E. Madjet, and H. S. Chakraborty, *Phys. Rev. A* **80**, 011201(R) (2009).  
 [26] A. Rüdél, R. Hentges, U. Becker, H. S. Chakraborty, M. E. Madjet, and J. M. Rost, *Phys. Rev. Lett.* **89**, 125503 (2002).  
 [27] M. E. Madjet and P. A. Hervieux, *Eur. Phys. J. D* **9**, 217 (1999).  
 [28] M. E. Madjet, H. S. Chakraborty, and J. M. Rost, *J. Phys. B* **34**, L345 (2001).  
 [29] O. Gunnerson and B. Lundqvist, *Phys. Rev. B* **13**, 4274 (1976).  
 [30] N. Rösch, O. Häberlen, and B. I. Dunlap, *Angew. Chem., Int. Ed. Engl.* **32**, 108 (1993).  
 [31] G. F. Bertsch, *Comput. Phys. Commun.* **60**, 247 (1990).  
 [32] U. Fano, *Phys. Rev. A* **124**, 1866 (1961).  
 [33] M. Ya. Amusia, A. S. Baltenkov, and L. V. Cherychva, *JETP Lett.* **87**, 200 (2008).